RESEARCH ARTICLE

WILEY PHOTOVOLTAICS

Minority carrier lifetime in indium doped silicon for photovoltaics

John D. Murphy[1] ⓘ | Alex I. Pointon[1] | Nicholas E. Grant[1] | Vishal A. Shah[1] | Maksym Myronov[2] ⓘ | Vladimir V. Voronkov[3] | Robert J. Falster[1]

[1] School of Engineering, University of Warwick, Coventry CV4 7AL, UK

[2] Department of Physics, University of Warwick, Coventry CV4 7AL, UK

[3] GlobalWafers, via Nazionale 59, 39012 Merano, Italy

Correspondence
John D. Murphy, School of Engineering, University of Warwick, Coventry CV4 7AL, UK.
Email: john.d.murphy@warwick.ac.uk

Abstract

For photovoltaics, switching the p-type dopant in silicon wafers from boron to indium may be advantageous as boron plays an important role in the light-induced degradation mechanism. With the continuous Czochralski crystal growth process it is now possible to produce indium doped silicon substrates with the required doping levels for solar cells. This study aims to understand factors controlling the minority carrier lifetime in such substrates with a view to enabling the quantification of the possible benefits of indium doped material. Experiments are performed using temperature-dependent Hall effect and injection-dependent carrier lifetime measurements. The recombination rate is found to vary linearly with the concentration of un-ionized indium which exists in the sample at room temperature due to indium's relatively deep acceptor level at 0.15 eV from the valence band. Lifetime in indium doped silicon is also shown to degrade rapidly under illumination, but to a level substantially higher than in equivalent boron doped silicon samples. A window of opportunity exists in which the minority carrier lifetime in degraded indium doped silicon is higher than the equivalent boron doped silicon, indicating it may be suitable as the base material for front contact photovoltaic cells.

KEYWORDS

dopant, indium, lifetime, light-induced degradation, photovoltaics, silicon

1 | INTRODUCTION

The vast majority of photovoltaic (PV) solar cells are made from boron doped p-type silicon substrates. Such substrates are potentially susceptible to light-induced degradation (LID) due to the formation of a recombination centre containing boron and oxygen,[1] which can result in cell conversion efficiency reductions of ~10% (relative). Oxygen in silicon usually originates from the silica crucibles which contain the melt. Whilst low oxygen concentrations can be achieved by modifying the Czochralski process with magnetic fields (~3 × 10^17 cm^−3)[2] or novel processes such as NeoGrowth (~4 × 10^17 cm^−3)[3], the production of such crystals is relatively expensive or immature. Float-zone silicon (FZ-Si) has lower oxygen concentrations than Cz-Si or mc-Si (usually <5 × 10^15 cm^−3) but comes with other lifetime stability issues probably due to complexes associated with intrinsic point defects[4] and is also much more expensive. Using n-type substrates is generally beneficial from the perspective of bulk lifetime,[5] but this requires modifications to

standard p-type cell processes such as diffusions, electrical contact schemes, and surface passivation.

Creation of p-type substrates by doping silicon with group III elements other than boron (such as aluminium, gallium, or indium) may provide a route to reducing or eliminating LID. Aluminium is unlikely to be a viable bulk dopant, as aluminium-oxygen complexes exhibit strong recombination activity.[6] Gallium doped silicon exhibits stable high lifetimes upon illumination[7,8] so could be a viable alternative. Indium doped silicon has been studied since the 1950s.[9] Historically, indium doped crystal growth research has been in the context of the development of infrared detectors[10,11] for which the challenge is to get a high concentration of indium. Crystal growth is challenging due to the relatively low segregation coefficient of indium,[10,12,13] evaporation of indium from the melt,[12] and the clustering or precipitation of indium at high concentrations.[11,12,14,15] Photovoltaic devices generally require lower levels of indium doping than infrared detectors, and recent work has shown that 200 mm diameter indium doped silicon wafers with PV-relevant doping levels can be grown on an industrial scale.[13] Passivated emitter and rear cells (PERC) made from indium doped silicon substrates have an efficiency of >20% even after exposure to light levels which would result in substantial LID in boron doped cells.[16] It is also noted that indium's relative scarcity is unlikely to limit the commercial deployment of indium doped silicon. Based on solar irradiance of 1000 Wm^{-2}, 1 TW of silicon PV peak capacity equates to 5×10^9 m^2 of 20% efficient silicon PV cells. If these are 180 μm thick, the required volume of silicon for 1 TW capacity is 9×10^5 m^3. The indium doping level will be ~10^{16} cm^{-3}, which is around 2×10^{-7} of the silicon volume, so the volume of indium required for this level of deployment is 0.18 m^3. The density of indium is 7310 kg/m^3, which means that only 1300 kg of indium is required for 1 TW peak of indium doped silicon deployment, which is a tiny fraction of the world's total indium reserves of >356 000 000 kg.[17]

The challenge with the deployment of indium doped silicon arises from indium's relatively deep acceptor level, which optical measurements reveal to be at $E_V + 0.15$ to $E_V + 0.16$ eV.[9,18-21] For shallow acceptors, such as boron, aluminium, and gallium, it is often reasonable to assume complete ionization at room temperature. With indium doping, this approximation is not valid, so not only does the doping level change with temperature, but the un-ionized indium has the potential to act as a recombination centre. The aim of this paper is to understand factors which control the minority carrier lifetime (henceforth just "lifetime") in indium doped silicon for PV applications. We use temperature-dependent Hall effect measurements to determine the concentration of ionized indium, and make injection-dependent lifetime measurements on the same material. We correlate lifetime measurements with indium levels to establish the relationship between lifetime and the levels of ionized and un-ionized indium. By analysing the injection dependence of the lifetime, we extract the relevant defect parameters and hence enable general parameterization of lifetime in indium doped silicon. As there are apparent conflicts in the literature regarding whether indium doped silicon itself experiences LID,[16,22-24] we perform LID

experiments. We compare the final lifetimes to those expected for boron doped silicon with equivalent doping and oxygen concentrations after complete boron-oxygen LID to assess the viability of indium doped silicon in PV applications.

2 | EXPERIMENTAL METHODS

Seven indium doped mono-crystalline silicon wafers grown by the continuous Czochralski process were studied. Samples for characterization were laser cut from 156 mm diameter pseudo squares, which were initially ~190 μm thick. Interstitial oxygen and, in some cases, substitutional carbon concentrations were measured by infrared spectroscopy in sections of the ingot from which the wafers used were taken. The maximum and minimum values measured are given in Table 1, and concentrations in the wafers studied lie in this range.

For Hall effect measurements, the Van der Pauw method with contacts at the corners of 10 mm × 10 mm square samples was used. Contacts were formed by evaporation of aluminium followed by a 10 min anneal at 450°C in a nitrogen atmosphere. Hall effect measurements were made from 100 K up to 320 K, which was the maximum operational temperature of the system.

The main set of samples for lifetime measurements (40 mm × 40 mm) first underwent a chemical etch which typically removed ~30 μm of material from each side. Samples were then subjected to room temperature superacid-derived surface passivation[25,26] which used a thin film formed from a solution of bis(trifluoromethane)sulfonimide (TFSI) dissolved in anhydrous 1,2-dichloroethane using a procedure described in detail by Grant et al.[25] The advantage of this scheme over dielectrics is that it avoids possible ambiguities associated with annealing, external gettering, and possible hydrogenation which typically occur with dielectric passivation.[27] We expect excellent surface passivation from the superacid-derived scheme and have previously shown surface recombination velocities (SRVs) of 2.7 ± 1 cms^{-1} for 1 Ωcm and 0.63 ± 0.07 cms^{-1} for 10 Ωcm boron doped silicon.[25] Lifetimes were measured at room temperature (~25°C) by photoconductance measurements conducted with a Sinton WCT-120 lifetime tester. Errors in lifetime measurements were taken as 5%, as guided by a reproducibility study.[28] Based on information in Table 1, it is noted that the level of compensation in some samples is as high as 2.2, which according to Schindler et al[29] would lead to a reduction in mobility of around 10%. This relatively small change is ignored in the measurement of lifetimes presented in this paper. Samples with superacid-derived passivation were also characterized by photoluminescence (PL) imaging[30] using a BT Imaging LIS-L1 PL system with a photon flux of 2.6×10^{17} cm^{-2} s^{-1}.

A second set of lifetime samples cut from the same indium doped wafers was used for LID experiments. Such experiments required surface passivation with better temporal stability than the superacid-derived scheme, and we opt for Al_2O_3 deposited by atomic layer deposition (ALD) rather than SiN_x as the latter has its own instabilities under illumination.[31,32] Float-zone silicon samples (360 μm thick, 2 Ωcm, n-type) were also passivated to demonstrate

TABLE 1 Details of the samples studied in this paper and their properties derived from fitting of Hall effect data

Sample	Superacid-Passivated Lifetime Sample Thickness [μm]	Interstitial Oxygen to DIN 50438/I (1995) [× 10^17 cm^-3] Minimum	Maximum	Substitutional Carbon [×10^15 cm^-3] Minimum	Maximum	Total In Concentration from Hall Fitting, N_a [×10^15 cm^-3]	Ionized In Concentration at 298 K, p_{298K} [×10^15 cm^-3]	Un-Ionized In Concentration at 298 K, $N_a - p_{298K}$ [×10^15 cm^-3]	Compensation from Hall Fitting, N_d [×10^15 cm^-3]
In-1	120	5.9	6.4	Not known	Not known	33	10.9	22	0.08
In-2	130	6.4	7.4	Not known	Not known	27	9.5	18	1.6
In-3	120	5.6	6.2	12.3	15.6	28	9.0	19	3.0
In-4	130	3.8	5.2	17.5	30.1	25	7.9	17	3.0
In-5	130	7.4	9.0	Not known	Not known	19	6.7	12	1.4
In-6	120	6.2	7.3	6.9	15.6	16	6.7	9.3	2.0
In-7	140	7.3	7.5	6.9	8.1	4.0	2.1	1.9	0.8

the stability of the surface passivation under illumination. Samples were subjected to a thorough surface preparation procedure involving a dip in HF (2%), an RCA 1 clean (H_2O, H_2O_2 (30%), NH_4OH (30%) in the ratio 5:1:1) at 75°C for 5 minutes, a dip in HF (2%), a tetramethylammonium hydroxide etch at 80°C for 10 minutes, a dip in HF (2%), an RCA 2 clean (H_2O, H_2O_2 (30%), HCl (37%) in the ratio 5:1:1) at 75°C for 10 minutes, and a final HF dip (2%). The samples, which were typically 180 μm thick after the pretreatment, were then pulled dry from the final HF dip (ie, no rinsing) and were immediately transferred to a Veeco Fiji G2 ALD system where they were rapidly put under vacuum to prevent surface oxidation. Al_2O_3 was deposited at 200°C using a plasma O_2 source and a trimethylaluminum precursor for 160 cycles to give films ~15 nm thick. The samples were then turned over, and the same deposition conditions were used to deposit Al_2O_3 on the other surface. To activate the passivation, a postdeposition anneal in air was performed in a quartz tube furnace at 450 ± 10°C for 30 minutes. LID experiments were performed using a halogen lamp to give a sample irradiance of approximately 1 Sun, and this resulted in the samples being heated up to 40 to 50°C during illumination.

3 | RESULTS AND ANALYSIS

3.1 | Hall effect data

The hole concentration calculated from the Hall effect experiments is shown in Figure 1. For consistency with several other Hall effect studies in indium doped silicon,[10,33-35] we take the Hall coefficient as unity. The hole concentration at 298 K (p_{298K}) is extracted from Figure 1 and is taken as the ionized indium concentration for analysis of lifetime data. Complete ionization of the indium acceptor is not
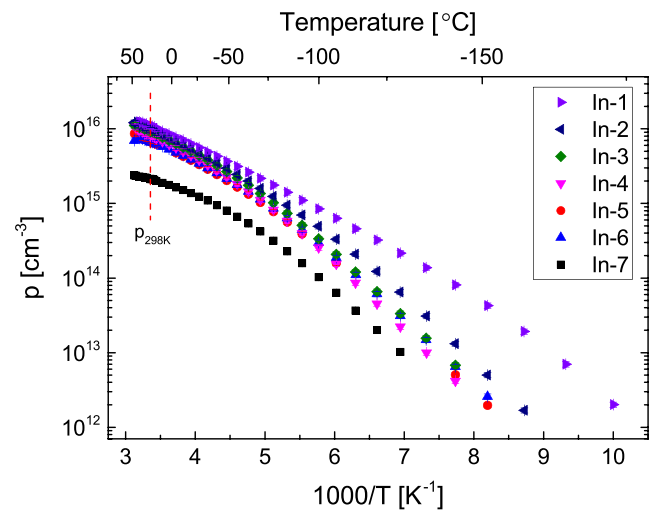

FIGURE 1 Carrier concentration versus temperature from Hall effect measurements. The values at 298 K were taken as the ionized indium concentrations for the lifetime measurements presented later [Colour figure can be viewed at wileyonlinelibrary.com]

achieved at our highest possible measurement temperature (320 K). A fit to the Hall effect carrier concentration data is therefore performed to give an estimation of the fully ionized indium concentration (N_a). By considering charge neutrality in a nondegenerate p-type semiconductor with majority acceptors above the valence band, it can be shown (eg, by Blakemore[36]) that

$$\frac{p(p + N_d)}{N_a - N_d - p} = p_1^* \tag{1}$$

where

$$p_1^* = gN_v \exp\left(-\frac{E_a}{kT}\right) \tag{2}$$

and where p is the hole concentration (temperature dependent), N_d is the total donor concentration, N_a is the total acceptor concentration, g is the spin degeneracy, N_v is the density of states in the valence band, E_a is the energy level of the acceptor above the valence band, k is Boltzmann's constant, and T is absolute temperature. It should be noted that the definition of p_1^* in Equation (2) is different to the definition of p_1 used in lifetime measurements later in this paper as it includes the degeneracy factor (g) which is commonly included for Hall effect studies. Rearranging Equation (1) and solving as a quadratic in p gives the positive root:

$$p = \frac{1}{2}\left[\left(\sqrt{(N_d + p_1^*)^2 - 4p_1^*(N_d - N_a)}\right) - (N_d + p_1^*)\right]. \tag{3}$$

Equation (3) is therefore used to fit the temperature-dependent hole concentration data from the Hall effect measurements assuming the main indium level is the only acceptor state. Figure 2 shows the results of this fitting for three samples. In all cases, we take $N_v = 1.95 \times 10^{15} \times T^{3/2}$ cm^{-3} [37] and $g = 0.25$ (based on Baron et al[33]). E_a is varied in the range 0.152 to 0.159 eV to achieve the best fit to the experimental data. The key parameters resulting from the fit are N_a (the total indium concentration) and N_d (the compensating donor concentration), and these are listed in Table 1 for all the samples. The un-ionized indium concentration at 298 K is calculated as $N_a - p_{298K}$ and is also shown in Table 1. The key point is that at room temperature there is a substantial concentration of both ionized and un-ionized indium in all samples, with the ionization level ranging from approximately 32% to 53%.

3.2 | Measured lifetime data

The measured lifetimes in as-received samples with superacid-derived passivation are plotted in Figure 3. The lifetime curves have similar injection dependences in all cases, which is indicative of the recombination occurring via the same processes, and this is analysed in more detail later. Figure 4 shows calibrated PL lifetime images of several indium doped samples taken with 1 Sun illumination. The average injection levels are approximately 8×10^{15} cm^{-3} for In-7, 4×10^{15} cm^{-3} for In-6, 2×10^{15} cm^{-3} for In-4, and 4×10^{14} cm^{-3} for In-1. These images demonstrate both the uniformity of the surface passivation and the uniformity of the bulk lifetime in the samples studied. Some silicon wafers contain annular striations, which are often associated with suboptimal crystal growth conditions.[38] There
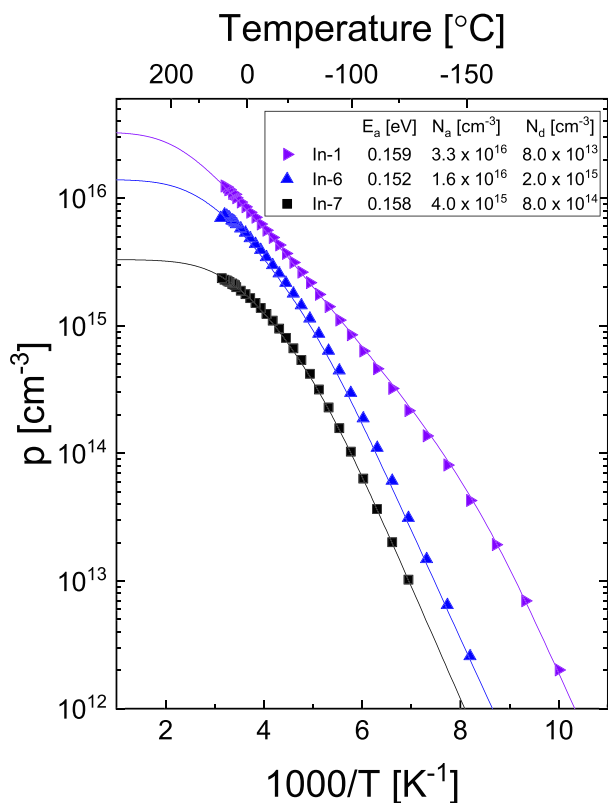
FIGURE 2 Carrier concentration versus temperature from Hall effect measurements in selected samples. The fits to the data were used to ascertain the total indium concentration in the samples. Key fit parameters for all samples are given in Table 1 [Colour figure can be viewed at wileyonlinelibrary.com]
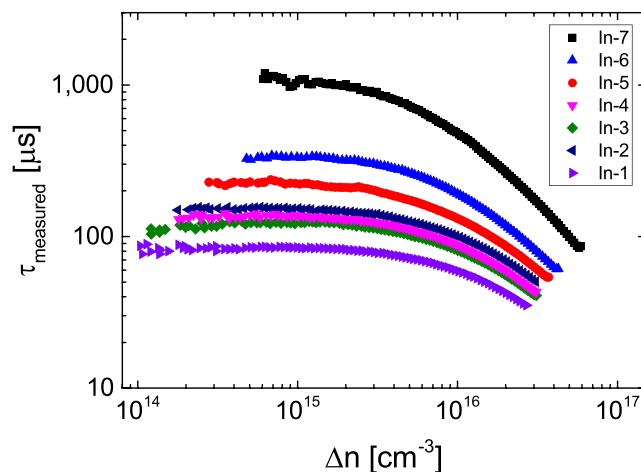
FIGURE 3 Measured lifetime versus excess carrier concentration in as-received indium doped silicon samples measured with superacid-derived surface passivation [Colour figure can be viewed at wileyonlinelibrary.com]
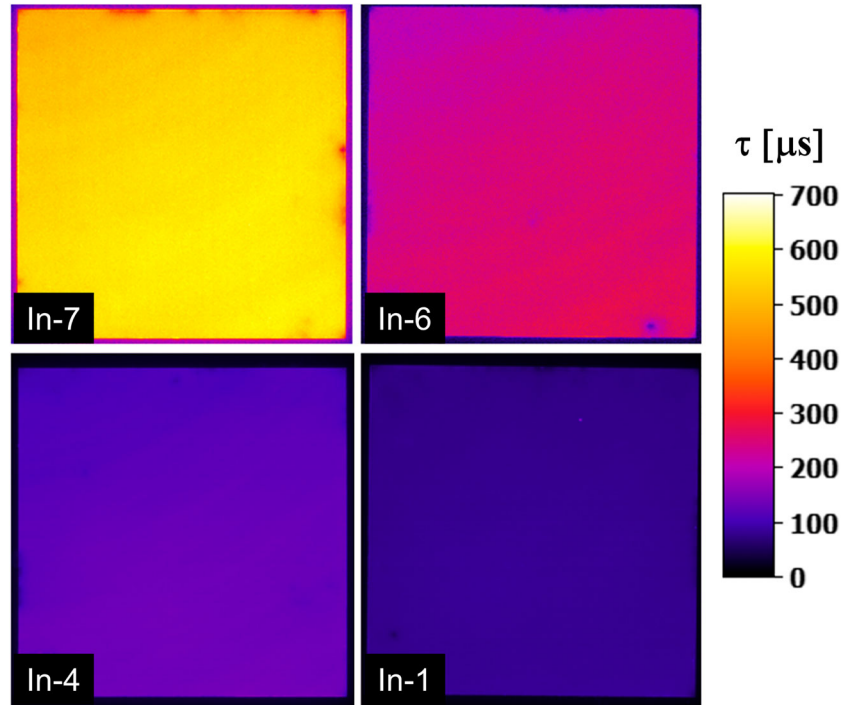
FIGURE 4 Calibrated PL lifetime images under 1 Sun illumination of selected as-received indium doped silicon samples (4 cm × 4 cm) measured with superacid-derived surface passivation. These images demonstrate the uniformity of both the surface passivation and the lifetime distribution in the sample [Colour figure can be viewed at wileyonlinelibrary.com]

is a slight hint of these in Sample In-7 (top left), but their impact on bulk lifetime appears to be fairly small in the samples studied.

3.3 | Correlation of recombination with indium

To establish a possible correlation between lifetime and indium doping, the intrinsic lifetime given by the parameterization of Richter et al[39] was removed from the measured lifetime according to

$$\tau_{residual} = \left(\frac{1}{\tau_{measured}} - \frac{1}{\tau_{intrinsic}}\right)^{-1}. \tag{4}$$

The residual lifetime, $\tau_{residual}$, will still include a small contribution from other recombination processes not related to indium, τ_{other}. Figure 5 shows the correlation between $\tau_{residual}$ and both the ionized (p_{298K}) and un-ionized ($N_a - p_{298K}$) indium concentrations at 10^{15} and 10^{16} cm^{-3} injections. There is an approximately linear relationship between recombination and un-ionized indium.

If the un-ionized indium acts as a recombination centre, then the recombination rate can be expressed according to

$$\frac{1}{\tau_{residual}} = \alpha_n(N_a - p_{298K}) + \frac{1}{\tau_{other}} \tag{5}$$

where α_n is the capture coefficient for electrons at the un-ionized indium centre (the capture coefficient is the product of the capture cross section and the thermal velocity). The linear fits to the black circles in Figure 5 are in accordance with Equation (5), and the gradients —which are equivalent to capture coefficients α_n—are given by $1.7 \pm 0.2 \times 10^{-12}$ and $2.4 \pm 0.3 \times 10^{-12}$ cm^3 s^{-1} for injection levels of 10^{15} and 10^{16} cm^{-3}, respectively. The corresponding intercepts

are given by 521 ± 154 and 1243 ± 261 s^{-1}. τ_{other} will be partly determined by surface recombination, so the intercepts from Figure 5 can be used to place an upper limit on the SRV, S, according to

$$S \leq \frac{W}{2\tau_{other}} \tag{6}$$

where W is the wafer thickness of around 130 μm. This analysis gives $S \leq 4$ cms^{-1} at 10^{15} cm^{-3} and ≤ 8.1 cms^{-1} at 10^{16} cm^{-3}. In a study of superacid-derived passivation of boron doped p-type silicon, it was found that $S < 2.7$ cms^{-1} for p-type silicon at 10^{15} cm^{-3} [25] so, either the surface passivation for these indium doped samples was not as good for some unknown reason, or there is a small amount of other bulk recombination in the samples.

Equation (1) at 298 K can be rewritten as

$$N_a = \frac{p_{298K}(p_{298K} + N_d)}{p_1^*} + N_d + p_{298K}. \tag{7}$$

Substituting Equation (7) into Equation (5) gives

$$\frac{1}{\tau_{residual}} = \alpha_n\left[\frac{p_{298K}(p_{298K} + N_d)}{p_1^*} + N_d\right] + \frac{1}{\tau_{other}}. \tag{8}$$

If the compensating donor concentration is small, then Equation (8) simplifies to

$$\frac{1}{\tau_{residual}} = \alpha_n\frac{p_{298K}^2}{p_1^*} + \frac{1}{\tau_{other}}. \tag{9}$$

Equation (9) implies that if recombination is via un-ionized indium, a quadratic dependence on recombination rate with p_{298K} is expected for samples which are not significantly compensated. The results
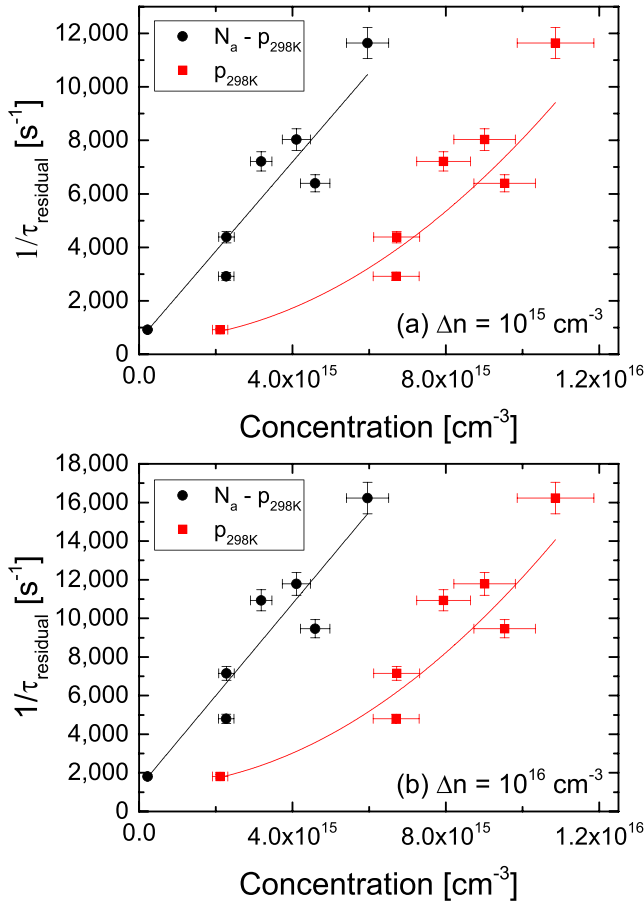
FIGURE 5 Residual recombination rate in as-received indium doped silicon samples versus concentration of either the un-ionized indium ($N_a - p_{298K}$) in black or the ionized indium concentration (p_{298K}) in red at an excess carrier of (a) 10^{15} cm^{-3} or (b) 10^{16} cm^{-3}. A linear fit is shown for un-ionized indium, and a quadratic fit is used for ionized indium [Colour figure can be viewed at wileyonlinelibrary.com]

presented in Figure 5 show approximate quadratic behaviour, with deviation from this most likely due to the level of compensation being non-negligible in some samples (see Table 1 and Equation (8)). The quadratic fits shown are performed by fixing the vertical axis intercepts to have the same values as the un-ionized indium linear fits. The fits used give values of $\frac{\alpha_n}{p_1^*}$ of 7.5 ± 0.8 × 10^{-29} cm^6 s^{-1} for 10^{15} cm^{-3} and 1.08 ± 0.14 × 10^{-28} cm^6 s^{-1} for 10^{16} cm^{-3}. Using the values of α_n extracted via Equation (5) previously gives the same value of p_1^* of 2.2 ± 0.4 × 10^{15} cm^{-3} for both injection levels. This can be used, in accordance with Equation (2), to extract E_a, the energy level of the defect responsible for the recombination relative to the valence band edge. Such an extraction requires knowledge of N_v and g. Perhaps surprisingly, there is a range of different values of N_v used in the literature, and a study by Green noted that using different parameters can result in energy level discrepancies of up to 30 meV.[40] Using the N_v values from Green[40] which are often used in lifetime studies, and $g = 0.25$ to be consistent with prior Hall effect studies,[33] gives E_a as 0.150 ± 0.04 eV. This is very similar to the known indium level. Using other values of N_v, such as those

used in older Hall studies (eg, by Schroder et al[34]), would give a lower value of E_a by around 30 meV, consistent with the findings of Green's work.

3.4 | Analysis of the lifetime injection dependence

To provide a deeper understanding of the recombination activity in indium doped silicon, the injection-dependent lifetime data were analysed using a linear version of Shockley-Read-Hall (SRH) statistics which has been described in detail previously.[41,42] For a p-type semiconductor, the lifetime is plotted as a function of the ratio of the total electron concentration to the total hole concentration. When appropriate, the lifetime curve can then be fitted with an integer number of independent SRH centres where the lifetime due to the ith SRH recombination centre varies according to

$$\tau_i = \frac{1}{\alpha_{ni}N_i}\left[1 + \frac{Q_i n_i}{p_0} + \frac{p_i}{p_0} + X\left(Q_i - \frac{Q_i n_i}{p_0} - \frac{p_i}{p_0}\right)\right]. \quad (10)$$

where α_{ni} is the capture coefficient for electrons, N_i is the concentration of the recombination centre, $Q_i = \frac{\alpha_{ni}}{\alpha_{pi}}$ where α_{pi} is the capture coefficient for holes, p_0 is the hole concentration (taken as p_{298K} here), and $X = \frac{n}{p} = \frac{n_0 + \Delta n}{p_{298K} + \Delta n}$. The variables n_i and p_i are the SRH densities for electrons and holes, respectively. By convention for lifetime measurements, the spin degeneracies used for SRH densities in Hall effect measurements (eg, for p_1^* in Equation (2)) are omitted, and so

$$n_i = N_c \exp\left(-\frac{(E_c - E_{Ti})}{kT}\right). \quad (11)$$

and

$$p_i = N_v \exp\left(-\frac{(E_{Ti} - E_v)}{kT}\right). \quad (12)$$

where N_c is the density of states in the conduction band, N_v is the density of states in the valence band, and E_{Ti} is the energy level of the trap relative the edge of the conduction band (E_c) or the valence band (E_v).

The residual lifetime from experiment can be fitted using an integer number of independent SRH centres each with lifetimes varying in accordance with Equation (10) combined according to

$$\tau_{residual} = \left(\sum_i \frac{1}{\tau_i}\right)^{-1}. \quad (13)$$

Figure 6 shows that the residual lifetime in indium doped samples plotted against X approximates to linear as X increases. In accordance with Equation (10), this suggests that one SRH centre dominates the recombination in indium doped silicon at relatively high X. At lower values of X, the lifetime curves in Figure 6 bend downwards, which implies the existence of at least one other SRH centre in the samples. To fit the curves shown in Figure 6, we adopt a two independent SRH centre approach and fit the data in accordance with Equation (13). We arbitrarily refer to the state dominant at high injection as State 1 and
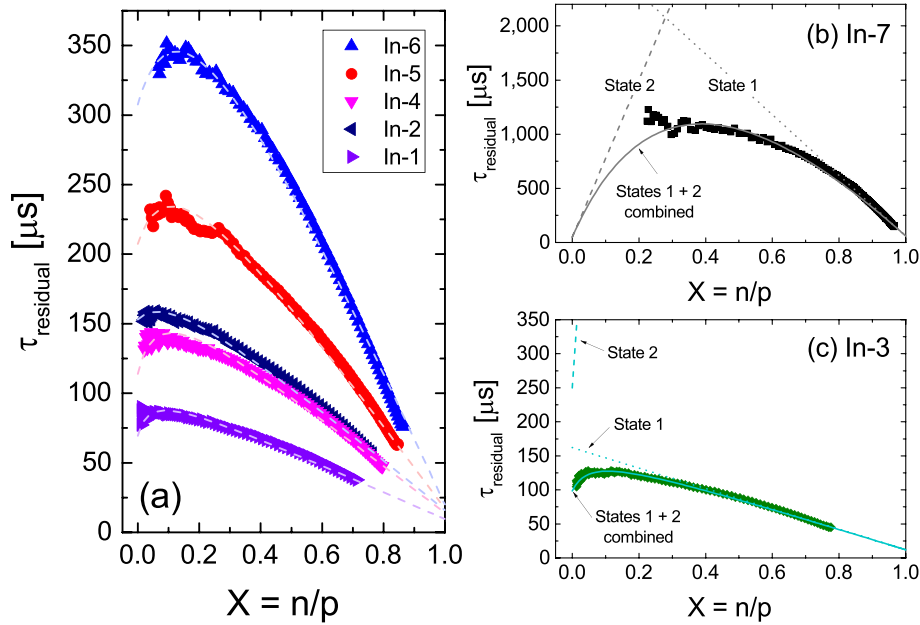
FIGURE 6 Residual lifetimes in as-received indium doped silicon samples plotted as a function of $X = n/p$. The two independent SRH states used to fit the data and their combined effect are shown in (b) for sample In-7 and (c) for sample In-3. Combined two state fits (but, for clarity, not their components) for the other samples are shown in (a) [Colour figure can be viewed at wileyonlinelibrary.com]

the other as State 2. In Figure 6(b) and (c), we show the two components used to fit the experimental data for two samples, and the fits shown in Figure 6(a) are the combination of these two states, but the individual states are not plotted for clarity. In order to fit the data, we have allowed the State 1 fit parameters to vary freely, but we have constrained the State 2 fit parameters to have the same value for all samples at the high injection limit where $X = 1$. Setting $X = 1$ in Equation (10) shows this so-called ambipolar lifetime limit to depend only on the concentration of the recombination centre and its capture coefficients for electrons and holes. This assumption is valid if the origin of State 2 is not related to indium but instead is related to a set of defects whose concentration is the same in all the samples studied, such as the remaining recombination centres at the surfaces of the samples after the superacid-derived surface passivation treatment.

State 1 is the dominant recombination centre in the indium doped silicon samples studied and, from Figure 6, it is clear that its concentration is dependent on the indium level in some way. A correlation between recombination rate and the un-ionized indium concentration was found in Figure 5. If State 1 is due to un-ionized indium, then taking the $X = 1$ limit of Equation (10) with $N_1 = N_a − p_{298K}$ gives

$$N_a - p_{298K} = \left(\frac{1}{\alpha_{n1}} + \frac{1}{\alpha_{p1}}\right)\frac{1}{\tau_{n1X \to 1}}. \tag{14}$$

where $\tau_{n1X \to 1}$ is the $X = 1$ limit of the State 1 fit to the experimental data. Figure 7(a) is a plot in accordance with Equation (14) which shows an approximate linear relationship between $N_a − p_{298K}$ and $1/\tau_{n1X\to1}$ with the fit shown having a gradient of $\frac{1}{\alpha_{n1}} + \frac{1}{\alpha_{p1}} = 1.96 \pm 0.21 \times 10^{11}$ scm^{-3}. This approximate linearity indicates that State 1 is most likely proportional to the un-ionized indium level.

Further evidence for State 1 being related to un-ionized indium can be gained for a more detailed analysis of the State 1 injection dependence. Differentiating Equation (10) for State 1 at 298 K with respect to X and normalizing this by the $X = 1$ limit gives the following expression which is independent of state density:

$$\frac{d\tau_{n1}}{dX}\bigg/\tau_{n1X\to1} = \frac{Q_1}{1+Q_1} - \frac{1}{p_{298K}}\left(\frac{Q_1 n_1 + p_1}{1 + Q_1}\right). \tag{15}$$

Figure 7(b) is a plot in accordance with Equation (15). Extrapolation of the fit shown gives a $1/p_{298K} = 0$ intercept of $\frac{Q_1}{1 + Q_1} = -1.17 \pm 1.20$, which implies $Q_1 < 0.036$. The gradient gives $\frac{Q_1 n_1 + p_1}{1 + Q_1} = 9.75 \pm 0.97 \times 10^{16}$ cm^{-3}. If State 1 is assumed to be closer to the valence band than the conduction band, then $p_1 > > Q_1 n_1$ and p_1 could lie in the range 8.8×10^{16} cm^{-3} to 1.1×10^{17} cm^{-3}. According to Equation (12) with N_v from Green,[40] this implies E_{T1} lies in the range 0.144 eV to 0.150 eV. This is similar to the energy level for indium in silicon measured by other techniques.[9,18-21]

3.5 | Degradation experiments

A series of experiments was performed to assess the degree to which indium doped silicon degrades under illumination. Whilst the superacid-derived passivation scheme used earlier in this paper provides very good initial passivation, it does not have sufficient temporal stability for use in LID experiments.[25,26] For this part of the study, different indium doped silicon samples, as well as n-type floatzone silicon controls, were passivated with Al$_2$O$_3$ and subjected to 1
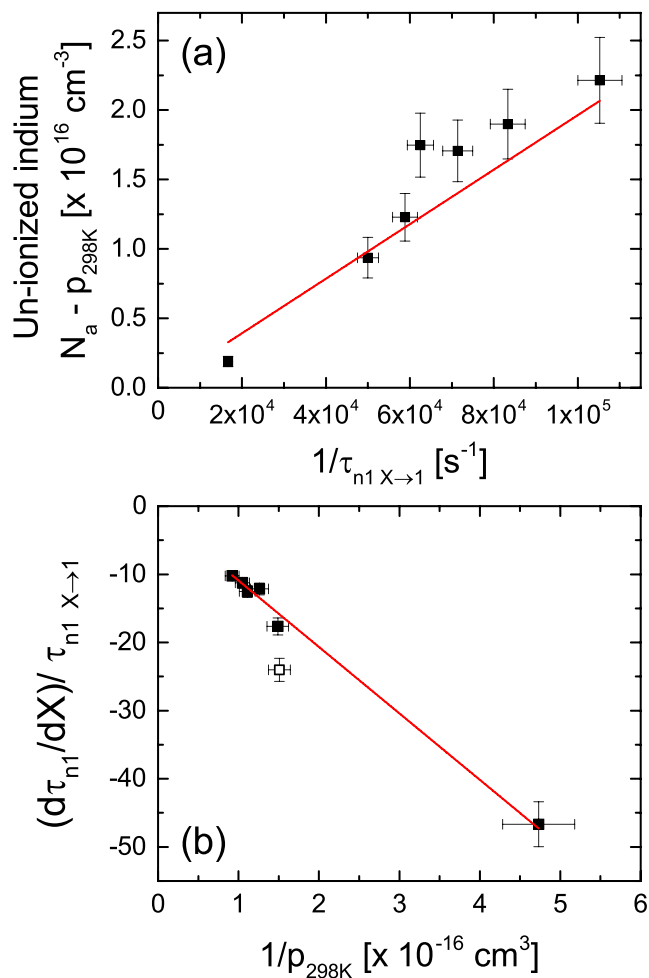
FIGURE 7 Plots relating to State 1 extracted from fitting the injection-dependent lifetime data for as-received indium doped silicon. Plot (a) shows the relationship between the $X = 1$ limit of the recombination rate and the un-ionized indium concentration. Plot (b) shows the relationship between the reciprocal of doping level and the fitted gradient for State 1 divided by its $X = 1$ lifetime limit. Gradients for the fits are given on the graphs, and the open symbol in plot (b) for sample In-6 was disregarded for fitting purposes [Colour figure can be viewed at wileyonlinelibrary.com]

Sun illumination. Significant lifetime degradation occurs in all indium doped samples, as shown by the data for sample In-7 in Figure 8(a). The degradation is not due to degradation of the surface passivation as measurements of float-zone silicon control samples also shown in Figure 8(a) show a stable lifetime within experimental error. In indium doped silicon, substantial lifetime degradation occurs in <1 second, with the lifetime then decaying to a steady state in a few minutes. As suggested by Möller and Lauer,[22] we find that a 200°C anneal reverses the LID, and, as shown in Figure 8(a), the lifetime then again degrades under illumination at approximately the same rate as on previous degradation cycles.

The motivation for using indium doped silicon would be to replace boron doped silicon which is well known to degrade under illumination.[43] It is therefore important to compare the degraded lifetimes in indium doped silicon with boron doped equivalents. For such a comparison, we use the parameterization of degraded lifetime in boron doped silicon from Bothe et al.[44] Noting the comments of Niewelt et al,[45] this provides a reasonable comparison to our data as it refers to the as-delivered state, and our samples did not undergo a high temperature diffusion step which can strongly affect the effective concentration of the recombination centre which forms under LID. In Figure 8(b), the lifetime for all the indium doped samples is plotted in the undegraded state ("U") after a 200°C anneal for 15 minutes, and the degraded state due to 1 Sun illumination for 1 hour ("D"). The lifetime in the degraded boron doped equivalent sample ("B") is also plotted using the parametrization of Bothe et al,[44] taking the oxygen concentration as the midpoint from the values in Table 1. Importantly, in all cases, the degraded lifetime is higher in the indium doped material than in the boron doped samples with a lifetime limited by the boron-oxygen defect.

4 | DISCUSSION

4.1 | Factors controlling lifetime

Our work clearly shows that the lifetime in as-received indium doped silicon is in some way dependent on the doping level of the sample. In Figure 3, we see a well-ordered family of lifetime curves. All the samples considered have relatively low doping levels and, even with excellent surface passivation, the lifetimes measured are well below those expected from intrinsic (Auger and radiative band-to-band) recombination.[39] The results presented in Figure 5 show that the lifetime varies linearly with the un-ionized indium concentration and with the square of the ionized indium concentration (subject to the limitations of this analysis in compensated material). Analysis in Figure 7(b) enables an energy level close to that expected for indium to be extracted from the injection-dependent lifetime data. We therefore conclude that the un-ionized indium gives rise to the main recombination centre which controls lifetime in our indium doped silicon samples.

In previous studies, indium doped silicon is often found to contain a shallower defect (sometimes called the "X-centre") at around $E_V + 0.11$ eV.[11,33,34,46,47] An initial study by Baron et al[33] found this defect to scale with the total indium concentration, and to exist in float-zone as well as Czochralski silicon thus probably ruling out the involvement of oxygen.[33] A later study showed a correlation with carbon concentration so it was concluded that the level was due to a substitutional carbon-indium pair,[47] and additional evidence for indium-carbon pairing comes from co-implantation studies.[48] For our samples, there is no clear evidence that the X-centre limits carrier lifetime at room temperature. We suspect the absence of X-centre effects arises because the relatively modern growth techniques used for our samples limit the incorporation of carbon. The carbon concentrations in our samples stated in Table 1 are at the lower end of the range studied by Baron et al.[47] Any effects of the X-centre in our samples are masked by the stronger recombination activity of the un-ionized indium.
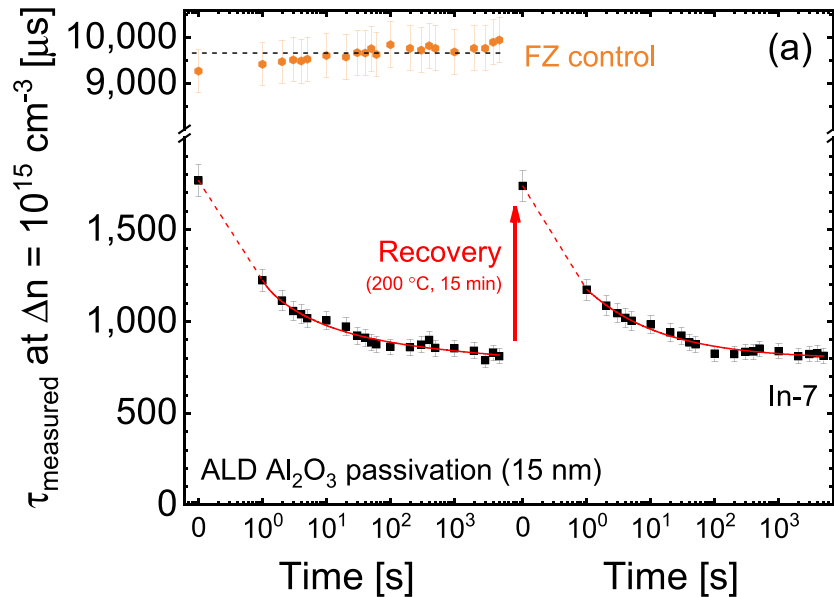
FIGURE 8 Measured effective lifetimes from LID experiments on ALD Al_2O_3 passivated indium doped samples. Graph (a) shows lifetime at an excess carrier density of 10^{15} cm^{-3} versus time under ~1 Sun illumination for sample In-7, showing the original lifetime can be recovered by a 15 min anneal at 200°C. The 2 Ωcm *n*-type float-zone (FZ) control sample does not degrade under illumination. Graph (b) shows the undegraded ("U") and degraded ("D") lifetimes in all the indium doped silicon samples studied. Also shown in graph (b) are the degraded lifetimes for boron-doped samples ("B") with the same doping level and oxygen concentration taken from the parameterization of Bothe et al.[44] Lifetimes in graph (b) are at an excess carrier density of $0.1 \times p_{298K}$ to facilitate direct comparison with Bothe et al's data [Colour figure can be viewed at wileyonlinelibrary.com]
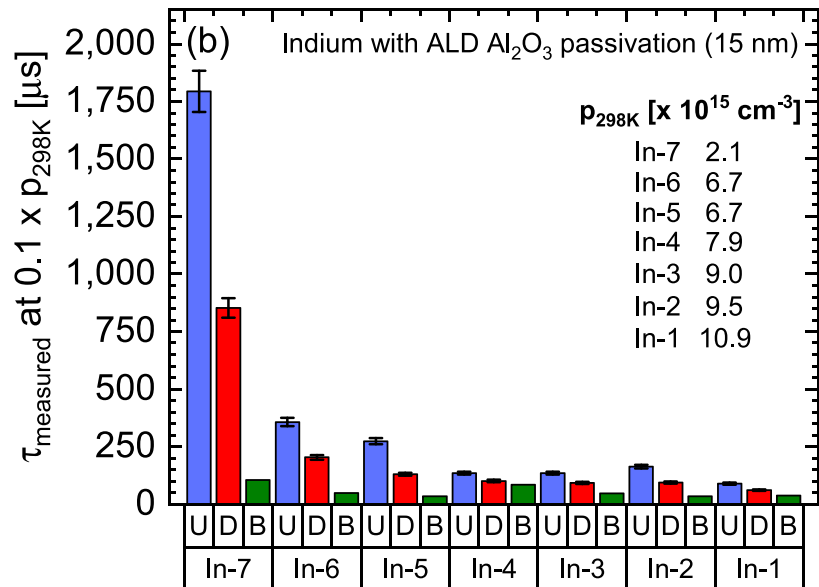
4.2 | Light-induced degradation

Our study has shown a clear degradation in lifetime in ALD Al_2O_3 passivated samples subjected to illumination (Figure 8). As the degradation does not occur in identically passivated float-zone control samples, we conclude that the bulk lifetime is degrading upon illumination and not the surface passivation. There are apparent conflicts in the literature regarding whether the properties of indium doped silicon change upon illumination, with some reporting stability and others a substantial degradation. Möller and Lauer found substantial lifetime degradation in indium doped samples, with degradation occurring much more slowly than in our samples.[22,23] A recent study by Cho et al found that passivated emitter rear cells (PERC) made from indium doped silicon do not degrade under illumination,[16] and Binns et al also concluded that only negligible lifetime degradation occurs in indium doped silicon upon light soaking.[24] Additionally, Schmidt and Bothe report limited results for indium doped silicon

in their LID studies and found the lifetime to be stable with illumination.[1] It is of course possible that others have not observed the LID effect that we have seen because it happens relatively quickly and it was simply missed.

The physical origin of the defect responsible for the LID in indium doped silicon is not currently known to us. Our initial results do not show a clear correlation with concentration of indium, oxygen, or carbon. We are currently working on understanding the mechanism of the LID effect, but, as with boron-oxygen-related LID,[43] this is likely to be a complex problem with variables such as bulk passivation, thermal history, and illumination conditions playing a role.

4.3 | Use of indium doped silicon in solar cells

This study has shown that indium doped silicon has the potential to offer higher carrier lifetimes than degraded boron doped equivalent

samples at room temperature, even after LID that occurs in indium doped samples. It is however noted that processes to regenerate boron doped silicon after boron-oxygen LID exist,[49,50] and application of similar processes to indium doped silicon may provide effective results. It is also important to note that a solar cell in service will typically operate above room temperature. Our Hall effect data (Figure 1) show that indium is not fully ionized at room temperature, so raising the temperature will increase the ionized indium concentration and hence reduce the un-ionized indium acting as a recombination centre. This means that the minority carrier lifetime should increase with temperature, but it is noted that to achieve a full temperature-dependent parameterization of lifetime in indium doped silicon it would be necessary to determine the temperature dependence of the electron and hole capture coefficients. Furthermore, because of the relatively deep acceptor state of indium, the effective doping level of an indium doped silicon substrate will change as the cell temperature changes. This is fundamentally unavoidable, and this variation may cause challenges for the optimization of other aspects of the cell manufacturing processes. This limitation also means that indium doped silicon may only be of use in front junction solar cells, such as PERC designs which have already been demonstrated.[16] Rear contact cells (eg, interdigitated back contact cells) require carrier lifetimes of several milliseconds or greater,[51] and even with the lowest indium level studied here (sample In-7), the un-ionized indium level limits the lifetime to below 2 ms (below 1 ms after LID).

5 | CONCLUSIONS

The electronic properties of indium doped silicon grown by the continuous Czochralski process have been studied systematically to understand factors which limit its minority carrier lifetime. The results of Hall effect experiments have been combined with those of injection-dependent lifetime measurements to understand the primary origin of the recombination activity in as-received samples. At room temperature, for typical PV substrate doping levels of 10^{15} to 10^{16} cm^{-3}, the un-ionized and ionized indium concentrations are of the same order of magnitude. The results show that the recombination activity is linearly dependent upon the concentration of un-ionized indium in the samples. Analysis of the injection dependence of the lifetime is consistent with a recombination centre at $E_v + 0.15$ eV, with an effective capture coefficient of around 2×10^{-12} cm^3 s^{-1}. Therefore, whilst the concentration of un-ionized indium is fundamentally very high at room temperature, its capture coefficient is very small, and this means that the lifetimes achieved in indium doped silicon are still suitable for some types of PV devices. A preliminary study has been performed into LID of indium doped silicon. The lifetime is found to degrade rapidly under illumination, but to stabilize at a level in most cases substantially higher than in equivalent boron doped samples. Thus, there exists a window of opportunity in which indium doped silicon can have a higher lifetime after degradation than boron doped silicon.

ORCID

John D. Murphy https://orcid.org/0000-0003-0993-5972
Maksym Myronov https://orcid.org/0000-0001-7757-2187

REFERENCES

1. Schmidt J, Bothe K. Structure and transformation of the metastable boron- and oxygen-related defect center in crystalline silicon. *Phys Rev B*. 2004;69(2):024107. https://doi.org/10.1103/PhysRevB.69.024107

2. Hoshikawa K, Kohda H, Hirata H, Nakanishi H. Low oxygen content Czochralski silicon crystal growth. *Jpn J Appl Phys*. 1980;19(1):L33-L36. https://doi.org/10.1143/JJAP.19.L33

3. Stoddard N, Russell J, Hixson EC, et al. NeoGrowth silicon: a new high purity, low-oxygen crystal growth technique for photovoltaic substrates. *Prog Photovolt Res Appl*. 2018;26(5):324-331. https://doi.org/10.1002/pip.2984

4. Grant NE, Markevich VP, Mullins J, et al. Permanent annihilation of thermally activated defects which limit the lifetime of float-zone silicon. *Phys Status Solidi A*. 2016;213(11):2844-2849. https://doi.org/10.1002/pssa.201600360

5. Macdonald D, Geerligs LJ. Recombination activity of interstitial iron and other transition metal point defects in p- and n-type crystalline silicon. *Appl Phys Lett*. 2004;85(18):4061-4063. https://doi.org/10.1063/1.1812833

6. Rosenits P, Roth T, Glunz SW, Beljakowa S. Determining the defect parameters of the deep aluminum-related defect center in silicon. *Appl Phys Lett*. 2007;91(12):122109. https://doi.org/10.1063/1.2789378

7. Glunz SW, Rein S, Knobloch J, Wettling W, Abe T. Comparison of boron- and gallium-doped p-type Czochralski silicon for photovoltaic application. *Prog Photovolt Res Appl*. 1999;7(6):463-469. https://doi.org/10.1002/(SICI)1099-159X(199911/12)7:6<463::AID-PIP293>3.0.CO;2-H

8. Dhamrin M, Hashigami H, Saitoh T. Elimination of light-induced degradation with gallium-doped multicrystalline silicon wafers. *Prog Photovolt Res Appl*. 2003;11(4):231-236. https://doi.org/10.1002/pip.482

9. Newman R. Optical properties of indium-doped silicon. *Phys Rev*. 1955;99(2):465-467. https://doi.org/10.1103/PhysRev.99.465

10. Scott W, Hager RJ. Solution growth of indium-doped silicon. *J Electron Mater*. 1979;8(5):581-602. https://doi.org/10.1007/BF02657080

11. Hobgood HM, Braggins TT, Sopira MM, Swartz JC, Thomas RN. Growth and characterization of indium-doped silicon for extrinsic IR detectors. *IEEE Trans Electron Devices*. 1980;27(1):14-23. https://doi.org/10.1109/T-ED.1980.19812

12. Yu X, Zheng X, Hoshikawa K, Yang D. Crystal growth of indium-doped Czochralski silicon for photovoltaic application. *Jpn J Appl Phys*. 2012;51:105501. https://doi.org/10.1143/JJAP.51.105501

13. Haringer S, Giannattasio A, Alt HC, Scala R. Growth and characterization of indium doped silicon single crystals at industrial scale. *Jpn J Appl Phys*. 2016;55(3):031305. https://doi.org/10.7567/JJAP.55.031305

14. Backenstoss G. Conductivity mobilities of electrons and holes in heavily doped silicon. *Phys Rev*. 1957;108(6):1416-1419. https://doi.org/10.1103/PhysRev.108.1416

15. Inoue K, Taishi T, Tokumoto Y, et al. Czochralski growth of heavily indium-doped Si crystals and co-doping effects of group-IV elements. *J Cryst Growth*. 2014;393:45-48. https://doi.org/10.1016/j.jcrysgro.2013.10.033

16. Cho E, Ok Y-W, Upadhyaya AD, et al. P-type indium-doped passivated emitter rear solar cells (PERC) on Czochralski silicon without light-induced degradation. *IEEE J Photovoltaics*. 2016;6(4):795-800. https://doi.org/10.1109/JPHOTOV.2016.2547578

17. Werner TT, Mudd GM, Jowitt SM. The world's by-product and critical metal resources part III: a global assessment of indium. *Ore Geol Rev*. 2017;86:939-956. https://doi.org/10.1016/j.oregeorev.2017.01.015

18. Blakemore JS. Photoconductivity in indium-doped silicon. *Can J Phys*. 1956;34(9):938-948. https://doi.org/10.1139/p56-104

19. Onton A, Fisher P, Ramdas AK. Spectroscopic investigation of group-III acceptor states in silicon. *Phys Rev*. 1967;163(3):686-703. https://doi.org/10.1103/PhysRev.163.686

20. Mason HJ Jr, Blakemore JS. Spectral dependence of photoconductivity in indium-doped silicon. *J Appl Phys*. 1972;43(6):2810-2817. https://doi.org/10.1063/1.1661600

21. Schelter W, Hell W, Helbig R, Schulz M. Optical properties of indium-doped silicon reinspected. *J Phys C Solid State Phys*. 1982;15(28):5839-5850. https://doi.org/10.1088/0022-3719/15/28/016

22. Möller C, Lauer K. Light-induced degradation in indium-doped silicon. *Phys Status Solidi Rapid Res Lett*. 2013;7(7):461-464. https://doi.org/10.1002/pssr.201307165

23. Möller C, Lauer K. A_{Si}-Si_i-defect model of light-induced degradation in silicon. *Energy Procedia*. 2014;55:559-563. https://doi.org/10.1016/j.egypro.2014.08.025

24. Binns MJ, Appel J, Guo J, et al. Indium-doped mono-crystalline silicon substrates exhibiting negligible lifetime degradation following light soaking. Proceedings of the 42nd IEEE Photovoltaic Conference; 2015. https://doi.org/10.1109/PVSC.2015.7355617.

25. Grant NE, Niewelt T, Wilson NR, et al. Superacid-treated silicon surfaces: extending the limit of carrier lifetime for photovoltaic applications. *IEEE J Photovoltaics*. 2017;7(6):1574-1583. https://doi.org/10.1109/JPHOTOV.2017.2751511

26. Pointon AI, Grant NE, Wheeler-Jones EC, Altermatt PP, Murphy JD. Superacid-derived surface passivation for measurement of ultra-long lifetimes in silicon photovoltaic materials. *Sol Energy Mater Sol Cells*. 2018;183:164-172. https://doi.org/10.1016/j.solmat.2018.03.028

27. Grant NE, Murphy JD. Temporary surface passivation for characterisation of bulk defects in silicon: a review. *Phys Status Solidi Rapid Res Lett*. 2017;11(11):1700243. https://doi.org/10.1002/pssr.201700243

28. Blum AL, Swirhun JS, Sinton RA, et al. Inter-laboratory study of eddy-current measurement of excess-carrier recombination lifetime. *IEEE J Photovoltaics*. 2014;4(1):525-531. https://doi.org/10.1109/JPHOTOV.2013.2284375

29. Schindler F, Schubert MC, Kimmerle A, et al. Modeling majority carrier mobility in compensated crystalline silicon for solar cells. *Sol Energy Mater Sol Cells*. 2012;106:31-36. https://doi.org/10.1016/j.solmat.2012.06.018

30. Trupke T, Bardos RA, Schubert MC, Warta W. Photoluminescence imaging of silicon wafers. *Appl Phys Lett*. 2006;89(4):044107. https://doi.org/10.1063/1.2234747

31. Sperber D, Graf A, Skorka D, Herguth A, Hahn G. Degradation of surface passivation on crystalline silicon and its impact on light-induced degradation experiments. *IEEE J Photovoltaics*. 2017;7(6):1627-1634. https://doi.org/10.1109/JPHOTOV.2017.2755072

32. Niewelt T, Selinger M, Grant NE, Kwapil WM, Murphy JD, Schubert MC. Light-induced activation and deactivation of bulk defects in boron-doped float-zone silicon. *J Appl Phys*. 2017;121(18):185702. https://doi.org/10.1063/1.4983024

33. Baron R, Young MH, Neeland JK, Marsh OJ. A new acceptor level in indium-doped silicon. *Appl Phys Lett*. 1977;30(11):594-596. https://doi.org/10.1063/1.89249

34. Thomas RN, Braggins TT, Hobgood HM, Takei WJ. Compensation of residual boron impurities in extrinsic indium-doped silicon by neutron transmutation of silicon. *J Appl Phys*. 1978;49(5):2811-2820. https://doi.org/10.1063/1.325161

35. Schroder DK, Braggins TT, Hobgood HM. The doping concentrations of indium doped silicon measured by Hall, CV, and junction breakdown techniques. *J Appl Phys*. 1978;49(10):5256-5259. https://doi.org/10.1063/1.324424

36. Blakemore JS. *Semiconductor Statistics*. New York, United States: Dover; 1987.

37. Voronkov VV, Voronkova GI, Batunina AV, Falster R. Advanced application of resistivity and Hall effect measurements to characterization of silicon. *ECS Trans*. 2009;25(3):25-34. https://doi.org/10.1149/1.3204391

38. Voronkov VV. The mechanism of swirl defects formation in silicon. *J Cryst Growth*. 1982;59(3):625-643. https://doi.org/10.1016/0022-0248(82)90386-4

39. Richter A, Glunz SW, Werner F, Schmidt J, Cuevas A. Improved quantitative description of Auger recombination in crystalline silicon. *Physical Review B*. 2012;86(16):165202. https://doi.org/10.1103/PhysRevB.86.165202

40. Green MA. Intrinsic concentration, effective densities of states, and effective mass in silicon. *J Appl Phys*. 1990;67(6):2944-2954. https://doi.org/10.1063/1.345414

41. Murphy JD, Bothe K, Krain R, Voronkov VV, Falster RJ. Parameterisation of injection-dependent lifetime measurements in semiconductors in terms of Shockley-Read-Hall statistics: an application to oxide precipitates in silicon. *J Appl Phys*. 2012;111(11):113709. https://doi.org/10.1063/1.4725475

42. Murphy JD, McGuire RE, Bothe K, Voronkov VV, Falster RJ. Minority carrier lifetime in silicon photovoltaics: the effect of oxygen precipitation. *Sol Energy Mater Sol Cells*. 2014;120:402-411. https://doi.org/10.1016/j.solmat.2013.06.018

43. Niewelt T, Schön J, Warta W, Glunz SW, Schubert MC. Degradation of crystalline silicon due to boron–oxygen defects. *IEEE J Photovoltaics*. 2017;7(1):383-398. https://doi.org/10.1109/JPHOTOV.2016.2614119

44. Bothe K, Sinton R, Schmidt J. Fundamental boron–oxygen-related carrier lifetime limit in mono- and multicrystalline silicon. *Prog Photovolt Res Appl*. 2005;13(4):287-296. https://doi.org/10.1002/pip.586

45. Niewelt T, Schön J, Broisch J, Mägdefessel S, Warta W, Schubert MC. A unified parameterization of the formation of boron oxygen defects and their electrical activity. *Energy Procedia*. 2016;92:170-179. https://doi.org/10.1016/j.egypro.2016.07.016

46. Scott W. Infrared spectra of new acceptor levels in indium or aluminum doped silicon. *Appl Phys Lett*. 1978;32(9):540-542. https://doi.org/10.1063/1.90121

47. Baron R, Baukus JP, Allen SD, et al. Nature of the 0.111eV acceptor level in indium doped silicon. *Appl Phys Lett*. 1979;34(4):257-259. https://doi.org/10.1063/1.90772

48. Scalese S, Italia M, La Magna A, et al. Diffusion and electrical activation of indium in silicon. *J Appl Phys*. 2003;93(12):9773-9782. https://doi.org/10.1063/1.1572547

49. Wilking S, Beckh C, Ebert S, Herguth A, Hahn G. Influence of bound hydrogen states on BO-regeneration kinetics and consequences for high-speed regeneration processes. *Sol Energy Mater Sol Cells*. 2014;131:2-8. https://doi.org/10.1016/j.solmat.2014.06.027

50. Walter DC, Lim B, Schmidt J. Realistic efficiency potential of next-generation industrial Czochralski-grown silicon solar cells after deactivation of the boron–oxygen-related defect center. *Prog Photovolt Res Appl*. 2016;24(7):920-928. https://doi.org/10.1002/pip.2731

51. Rahman T, To A, Pollard ME, et al. Minimising bulk lifetime degradation during the processing of interdigitated back contact silicon solar cells. *Prog Photovolt Res Appl*. 2018;26(1):38-47. https://doi.org/10.1002/pip.2928